
**Combustion Science and Technology**
Publication details, including instructions for authors and subscription information:
http://www.informaworld.com/smpp/title~content=t713456315

# Disturbance Field Characteristics of a Transversely Excited Burner

Jacqueline O'Connor[a]; Tim Lieuwen[a]
[a] School of Aerospace Engineering, Georgia Institute of Technology, Atlanta, Georgia, USA

Online publication date: 19 February 2011

**To cite this Article** O'Connor, Jacqueline and Lieuwen, Tim(2011) 'Disturbance Field Characteristics of a Transversely Excited Burner', Combustion Science and Technology, 183: 5, 427 — 443
**To link to this Article: DOI:** 10.1080/00102202.2010.529478
**URL:** http://dx.doi.org/10.1080/00102202.2010.529478

*Combust. Sci. and Tech.*, 183: 427–443, 2011

ISSN: 0010-2202 print/1563-521X online
DOI: 10.1080/00102202.2010.529478

Taylor & Francis
Taylor & Francis Group

# DISTURBANCE FIELD CHARACTERISTICS OF A TRANSVERSELY EXCITED BURNER

**Jacqueline O'Connor and Tim Lieuwen**
*School of Aerospace Engineering, Georgia Institute of Technology, Atlanta, Georgia, USA*

***Transverse acoustic instabilities in premixed, swirl-stabilized flames are an important problem in low $NO_x$ combustors. Transverse excitation of swirling flames involves complex interactions between acoustic waves and fluid mechanic instabilities. This paper presents high-speed PIV characterization of the flow field characteristics of a swirling, annular jet under reacting and nonreacting conditions. These data show that the flame response to transverse acoustic excitation is a superposition of acoustic and vortical disturbances that fluctuate in both the longitudinal and transverse direction. In the nozzle near-field region, the disturbance field is a complex superposition of short wavelength and convecting vortical disturbances, as well as longer wavelength transverse and longitudinal acoustic disturbances. Very near the nozzle, distinct vortical structures are evident that are associated with the separating inner and outer annulus shear layers. Their relative phasing on the left and right side of the burner annulus changes by 180° under conditions where the burner centerline is nominally at a transverse acoustic velocity node and antinode. These suggest that the dominant excited instability mode of the annular jet changes from axisymmetric to helical as the structure of the acoustic mode shape changes. Farther downstream, these structures disappear rapidly and the disturbance field is dominated by the longer wavelength, transverse acoustic field.***

***Keywords***: Combustion instabilities; Flame-acoustic interactions; Premixed flames



## INTRODUCTION

The objective of this study is to improve understanding of transverse combustion instabilities in premixed combustors. Such combustion instabilities are a common problem encountered in rocket and air-breathing engine development programs. The coupling of resonant acoustics in the combustion chamber and heat release fluctuations from the flame (Rayleigh, 1896) can cause structural damage, and decrease operational flexibility and performance. In particular, instabilities have caused major challenges in the development of lean, premixed combustors used in low $NO_x$ gas turbines (Lieuwen and Yang, 2005).

Transverse instabilities have been discussed frequently in the afterburner (Elias, 1959; Kaskan and Noreen, 1955; Macquisten and Dowling, 1995; Rogers

Received 13 July 2010; revised 15 September 2010; accepted 29 September 2010.
Address correspondence to Jacqueline O'Connor, Aerospace Combustion Lab, 635 Strong St., Atlanta, GA 30318. E-mail: joconnor6@gatech.edu

and Marble, 1956), solid rocket (Karnesky et al., 1975; Price, 1992), and liquid rocket literature (Berman and Logan, 1952; Davis and Chehroudi, 2006; Ellis et al., 2005; Harrje and Reardon, 1972; Marshall et al., 2006; Richecoeur et al., 2006). For low $NO_x$ gas turbines, most of the work over the last two decades has focused on the longitudinal instability problem (Alemela et al., 2010; Hield et al., 2009; Lawn et al., 2004; Reddy et al., 2006). Significantly less work has been done on the analysis and characterization of transverse instabilities for gas turbine type applications, typically characterized by a swirling, premixed flame (Hauser et al., 2010; Morgans and Stow, 2007; Schuermans et al., 2006; Staffelbach et al., 2009; Stow et al., 2001; Wolf et al., 2009; O'Connor et al., 2010). There are, however, two key application areas where transverse acoustic oscillations are of significant practical interest. The first occurs in annular combustion systems, such as the instabilities in the Solar Mars 100, Alstom GT24, GE LM6000, Siemens V84.3A, and other engines (Krebs et al., 2005; Sewell et al., 2005; Smith et al., 2005; Wolf et al., 2009). Because of the larger length scales involved, these instabilities often occur at the lower frequencies (e.g., 100 s of Hertz) that are typical of the longitudinal oscillations observed in can combustion systems. While these modes cannot typically be simulated without the full annulus, several of these studies report the results of longitudinal instability tests obtained on single nozzle rigs scaled to have similar longitudinal acoustic frequencies as the observed transverse instabilities (Cohen and Proscia, 2005; Krebs et al., 2005; Mongia et al., 2005). The second application where transverse instabilities are of interest is the higher frequency transverse oscillations encountered in can combustion systems. These instabilities occur at relatively high frequencies (e.g., in the 1–5 kHz range) and scale with the combustor can diameter. While relatively little treatment of these high frequency oscillations can be found in the technical literature, there is significant discussion of them in the gas turbine operator/user community—see Combined Cycle Journal (Schwieger, 2007) or Sewell and Sobieski's (2005) chapter in *Combustion Instabilities in Gas Turbine Engines*.

Transverse acoustic oscillations in combustors introduce a variety of new coupling processes and disturbance field phenomena relative to longitudinal modes. The focus of the next two sections is to elucidate these differences. In essence, the key problem of interest is the manner in which the flame responds to oscillations in flow velocity. This is referred to as the velocity coupled response mechanism (Birbaud et al., 2007; Hemchandra et al., 2010; Poinsot et al., 2006; Preetham et al., 2008; Schadow and Gutmark, 1992), to be distinguished from the also important fuel/air ratio coupling (Birbaud et al., 2008; Venkataraman et al., 1999;) mechanism, or the probably negligible pressure coupling mechanism (Ducruix et al., 2003). Flow oscillations lead to flame wrinkling that, in turn, causes oscillations in flame surface area and rate of heat release.

While acoustic flow oscillations can directly excite the flame, they also excite organized flow instabilities associated with shear layers, wakes, or the vortex breakdown bubble (Cala et al., 2006; Lacarelle et al., 2009; Syred, 2006). Taken together, there are a number of potential sources of flow disturbances that can lead to heat release oscillations. Two of these sources are directly acoustic in origin–transverse acoustic motions associated with the natural frequencies/mode shapes of the combustion system, and longitudinal oscillations in the nozzle due to the oscillating pressure difference across the nozzle. Results from simulations by Staffelbach et al. (2009)

suggest that it is these longitudinal mass flow oscillations that most significantly control the flame response to the imposed transverse disturbance.

Studies suggest that it is vortical flow oscillations that most significantly control the flame's heat release response (Ghoniem and Krishnan, 1989; Huang et al., 2003; Thumuluru et al., 2007). In other words, acoustic oscillations excite flow instabilities that, in turn, excite the flame. As such, the receptivity of these flow instabilities to both transverse and longitudinal acoustic oscillations must be considered. For example, consider the convectively unstable shear layers, which form tightly concentrated regions of vorticity through the action of vortex rollup and collective interaction (Ho et al., 2006). The transverse acoustic oscillation will disturb them in both normal and parallel directions. Normally incident transverse acoustic oscillations will push the shear layers from side to side in a flapping manner, while parallel incidence will graze over them. In contrast, longitudinal oscillations will lead to an axially oscillating core flow velocity that will excite an oscillation in shear layer strength (Thumuluru and Lieuwen, 2009; Wang et al., 2005). Other literature on the response of wakes and swirling flows to longitudinal and transverse excitation can be found in several references (Huang and Yang, 2009; Lacarelle et al., 2009; Shtork et al., 2008).

These disturbance modes are difficult to separate in complicated geometries and all play some role in exciting the flame. Although the initial disturbance is transverse, the disturbance velocity field that is created in the region of the flame is highly three-dimensional (Staffelbach et al., 2009; Wolf et al., 2009). This is significant in that the flame will experience a varying type of disturbance along its length. For example, a point in the middle of the flame may experience a strong transverse acoustic excitation source locally, as well as the disturbance from a vortex that was excited at the nozzle exit and has convected downstream. Complex interactions like these are difficult to separate, and it is one of the goals of this work to understand these characteristics of the disturbance field.

Having discussed some basic features of the transverse forcing problem, we conclude this section with an overview of the rest of this paper. Two-dimensional characterization of the velocity disturbance field in a transversely forced, swirl-stabilized flame is obtained from a time-resolved particle image velocimetry (PIV; Boxx et al., 2010). We first explain the experimental setup and give an overview of the diagnostics and data analysis tools used. Next, the disturbance field is characterized using several metrics to capture the different types of disturbances found in the region of the flame. Finally, several conclusions are drawn as to the underlying physics of the disturbance field and the effect of the velocity disturbance field on the flame behavior.

## EXPERIMENTAL FACILITY AND DATA ANALYSIS

The experimental facility is a single nozzle burner that was designed to support acoustic modes in the combustion chamber that are dominantly transverse in character, see Figure 1. The inner chamber dimensions are $1.14 \times 0.36 \times 0.08$ m, with the long dimension in the transverse direction. This configuration mimics the shape of an azimuthal mode in an annular combustor whose width is small relative to the radius, an approximation that is true in all commercial systems. The transverse

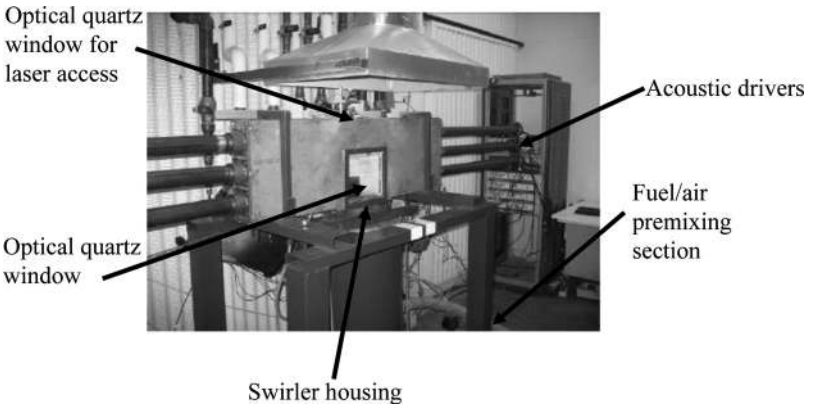


**Figure 1** Tunable transverse forcing combustion facility.



acoustic field is produced by two sets of drivers on either side of the combustor. Each driver sits at the end of an adjustable tube that allows for acoustic tuning to optimize control authority at the desired excitation frequency. By changing the phase between the signals driving each side of the combustor, different wave patterns, both standing and traveling waves, can be created inside the combustor. When the drivers are forced in phase, a pressure antinode and velocity node are created at the center of the experiment in the flame region. When the drivers are forced out of phase, a pressure node and velocity antinode are created at the center. The resulting flame response from these two forcing configurations is significantly different. These basic acoustic features and the axially uniform nature of the transverse disturbance field were verified by mapping out the disturbance field under no flow, nonreacting conditions.

The annular nozzle passage has a swirler with 12 angled blades with a 45° pitch and a 5.08 cm centerbody. The outer diameter of the swirler annulus is 3.18 cm and the inner diameter is 2.21 cm. The nozzle configuration, including the mode shapes around the nozzle for different acoustic forcing conditions, is shown in Figure 2. The average flame shape can also be seen in Figure 2; the flame is a V-flame stabilized in the inner shear layer.

Typical measured transverse velocities along the nozzle centerline are plotted in Figure 3 for in- and out-of-phase forcing, showing how it has small and large values, respectively. The nonzero value of the transverse velocity observed for the in-phase case is likely due to slight imbalances in excitation amplitudes of the left and right speakers.

PIV is used to measure the velocity field and the flame edge. The laser is a Litron Lasers Ltd. LDY303He Nd:YLF laser with a wavelength of 527 nm and a 5 mJ/pulse pulse energy at the 10 kHz repetition rate used for these experiments. The Photron HighSpeed Star 6 camera has a $640 \times 448$ pixel resolution with $20 \times 20$ micron pixels on the sensor at a frame rate of 10 kHz. Velocity field calculations were performed using DaVis 7.2 software from LaVision. A total of 500 velocity fields were obtained at each test condition, using 30 and 15 μs between laser shots at the bulk approach velocities of 10 and 40 m/s, respectively.

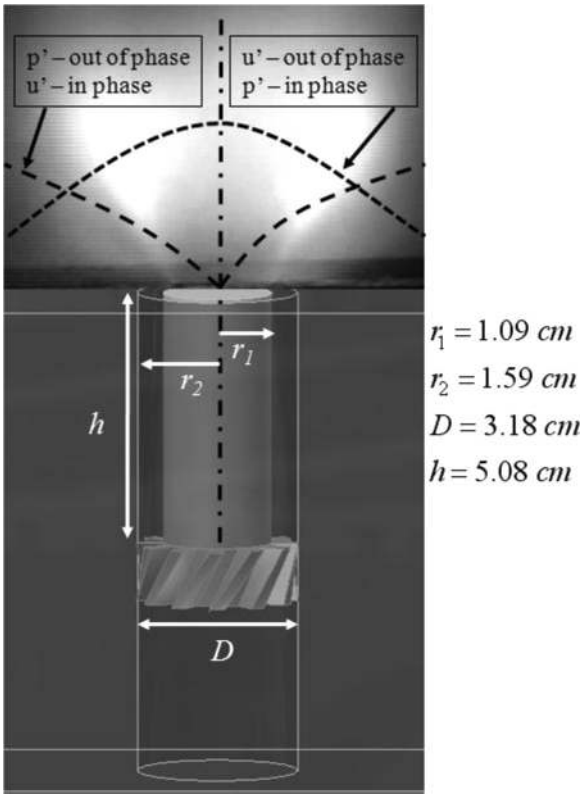


**Figure 2** Nozzle configuration, flame shape, and acoustic velocity and pressure perturbations for in- and out-of-phase acoustic forcing, from the side view (acoustic waves not shown to scale); 3.2 cm separate the base of the swirler with the settling chamber, which has a diameter of 40.6 cm and a length of 71.1 cm.



Several methods were used to process the data. Since the high-speed PIV system produces time-resolved velocity fields, spectral analysis was used in much of this study. First, spectra were calculated for each point in space in the velocity and vorticity fields. To calculate the coherent fluctuations, the amplitude and phase of the Fourier transform of the velocity, $\hat{A}(x)$ and $\varphi(x)$, were then used to harmonically reconstruct a time-domain flow field at the forcing frequency using the relation:

$$\hat{u}(\vec{x}, t) = \mathrm{Re}\left[\hat{A}(\vec{x})e^{-i(\omega t+\varphi(\vec{x}))}\right] \tag{1}$$

Hatted variables, such as the velocity in Eq. (1), are referred to as harmonically reconstructed quantities. Second, spatially averaged time-varying velocities were calculated in both the axial and transverse directions at the nozzle in order to compare the magnitude of the fluctuations in different directions. The calculation of spatially averaged transverse velocity is calculated along the centerline of the flow, across a length of one nozzle diameter. The axial velocity fluctuation is spatially averaged

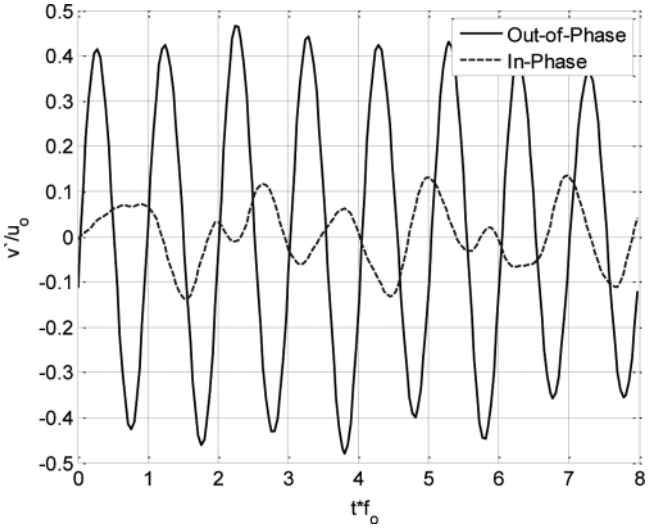


**Figure 3** Spatially averaged transverse velocity fluctuations along the nozzle centerline for 400 Hz acoustic forcing at 10 m/s, nonreacting flow.



about half the annular burner area for the right and left sides of the burner. These formulae are shown in Eq. (2). The signals are filtered using a second order Butterworth bandpass filter at ±200 Hz around the forcing frequency.

$$\bar{u}(t) = \frac{2\pi \int_{r1}^{r2} u(x=0,r,t) r dr}{2\pi(r_2^2 - r_1^2)}, \quad \bar{v}(t) = \frac{1}{D}\int_0^D v(x, r=0, t) dx \tag{2}$$

All results are shown in nondimensional form. The velocities are normalized by the bulk approach flow velocity, $m/\rho A$ (where $\rho$ and $A$ denote approach flow density and annulus area), the spatial coordinates by the nozzle outer diameter, $D$, time by the inverse of the forcing frequency, $1/f_o$, and the vorticity by the bulk velocity divided by the annular gap width, $U_o/(r_2 - r_1)$.

## RESULTS AND DISCUSSION

This section is organized by first discussing the time-averaged flow features, then the qualitative features of the unsteady flow, and finally the quantitative characteristics of the unsteady flow. The data presented here was selected from a larger set that includes flow velocities of 10, 15, 20, and 40 m/s; forcing frequencies of 400, 800, and 1200; 15 acoustic forcing amplitudes (transverse velocity amplitudes from 0 to 40% of the mean flow velocity); and equivalence ratios from 0.7–0.9 with natural gas as a fuel. The specific nonreacting data presented here is from the 10 and 40 m/s cases, and is all at 400 Hz, a transverse resonant frequency of the combustor system. The reacting data presented here was taken at a flow velocity of 10 m/s and an

equivalence ratio of 0.85. Although it is not possible to present the full set of test data here, the results that are presented show the representative coupling physics that was observed from analysis of the full data set. Additional discussion can be found in O'Connor et al. (2010).

The time-averaged axial velocity and vorticity fields for a nonreacting and reacting flow are plotted and compared in Figure 4. Several commonly observed differences in flow structure are evident between the nonreacting and the reacting flows. First, the spreading angle of the annular jet is greater in the reacting case, presumably because of the widening of the vortex breakdown bubble, which is shown in Figure 4. Second, the size and aspect ratio of the vortex breakdown region change significantly between the two cases. In the reacting case, the bubble has elongated and simultaneously become wider.

The response of the swirling flow to transverse acoustic excitation results in a highly multidimensional disturbance field. In general, the disturbances are of two types, acoustic and vortical. The acoustic disturbances propagate at the speed of sound and, in this case, set up a dominantly transverse standing wave with weak transverse phase variations. In addition, vortical disturbances excited by the acoustic motion at the nozzle exit convect downstream at the local flow velocity. These vortical disturbances induce fluctuations in both the axial and the transverse velocity. As a result, the transverse velocity fluctuations are a superposition of both the acoustic and the vortical motion.

These two types of disturbances, acoustic and convecting, can be visualized when considering the coherent disturbances, or the disturbance at the forcing frequency. Spectral analysis shows that both the acoustic and convecting motions respond very clearly at the forcing frequency with a much lower broadband noise floor. Figure 5 illustrates an overlay of the harmonically reconstructed velocity vectors (consisting of both acoustic and vortical disturbances) and isocontours of the vorticity fluctuations. While similar trends were seen for all the flow velocities measured in this study, the highest velocity case is shown here as the inner and outer shear layers are most clearly distinguished from each other. Only the harmonically reconstructed fluctuations at the forcing frequency is shown.



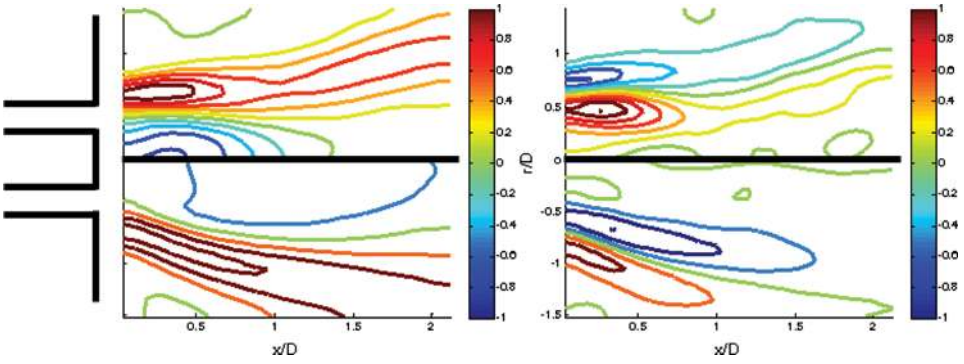


**Figure 4** Time-averaged axial velocity (left) and vorticity (right) in nonreacting (top) and reacting (bottom) flows. Bulk velocity is $U_o = 10\,\mathrm{m/s}$.

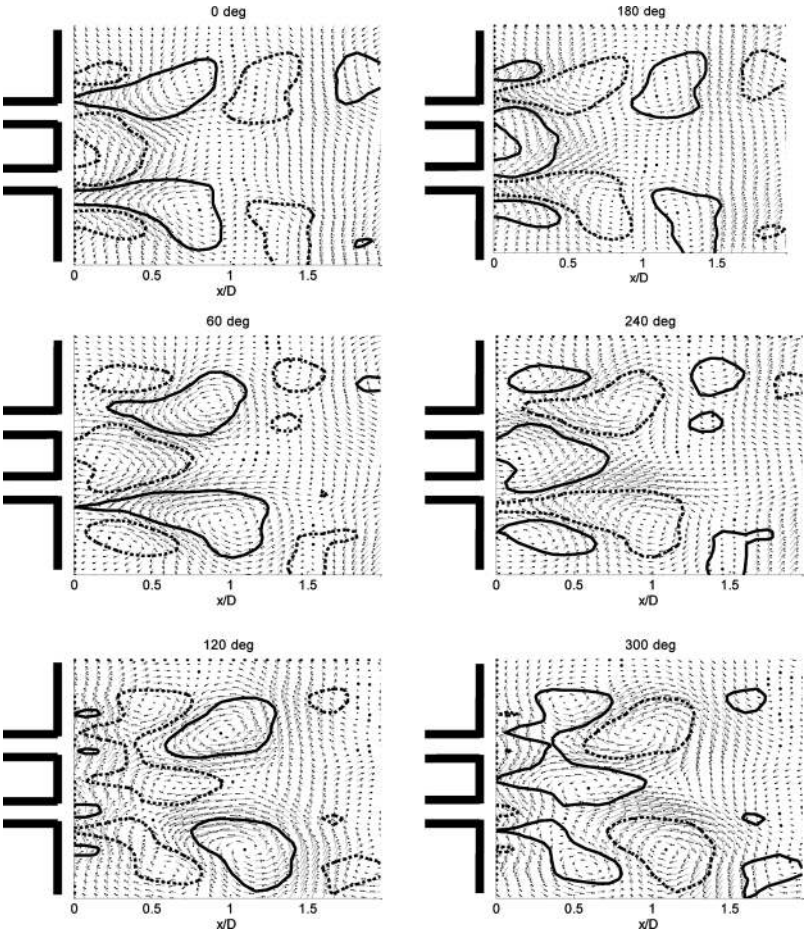


**Figure 5** Harmonically reconstructed velocity and vorticity fluctuations for $f_o = 400\,\text{Hz}$ out-of-phase acoustic forcing, nonreacting flow at $U_o = 40\,\text{m/s}$ bulk velocity. The dotted and solid vorticity isocontours denote values of $\omega U_o/(r_2 - r_1) = -0.1$ and 0.1, respectively.



Several physical processes are evident over the six phases pictured here. First, transverse fluctuation of the flow is dominant from approximately one diameter downstream to the end of the image. Second, transverse flapping of the jet region is evident. Finally, the unsteady formation and downstream convection of vorticity is present. The unsteady vorticity is generated in the two annular shear layers and rolls up into larger structures in the separating region associated with the inner and outer recirculation zones. While two counter-rotating regions of vorticity fluctuation are clearly evident at the annular slot exit, see Figure 5 at 0°, they subsequently interact farther downstream and only a single vorticity fluctuation region remains, located in the jet core (see Figure 5 at 120°).

Both vortical and acoustic disturbances are clearly seen in these plots. Vortical disturbances originate at the nozzle exit, and induce a dominantly axial motion in the

shear layer and a dominantly transverse motion in the jet core. Also evident from these plots is that the motions in adjacent shear layers oscillate out of phase with each other. As the axial velocity disturbance in the inner left shear layer rises at 0°, it falls in the inner right shear layer. Furthermore, the motions on the left side of the annulus are out of phase with those on the right side. This is apparently due to the almost 180° phase change of the pressure (note that the centerline is a pressure node for the out-of-phase acoustic forcing), a feature discussed subsequently.

The fluctuating vorticity also induces a transverse motion along the jet core, which is superposed with the periodic transverse acoustic motion that can be seen as the rise, fall, and downstream convection of the transverse velocity disturbances throughout the series of plots. These effects can be seen quantitatively in Figures 6a, 6b, and 6c, where the harmonically reconstructed vorticity, axial velocity, and transverse velocity fluctuations, respectively, are plotted along the jet and shear layer centerlines.

Figure 6a shows the fluctuation of coherent vorticity along the jet centers. The top and bottom subplots show the left and right jets, respectively.



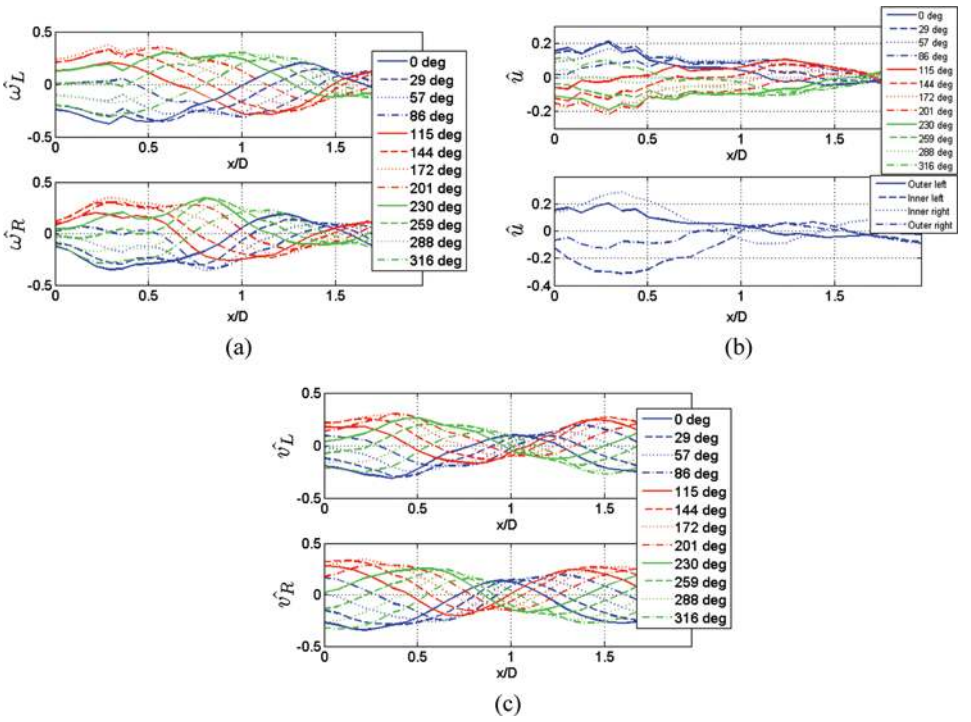


**Figure 6** Harmonically reconstructed (a) vorticity fluctuations along the left (top) and right (bottom) sides of the jet; (b) axial velocity fluctuations along the outer left shear layer across several phases (top), and across all four shear layers at 0° (bottom); and (c) transverse velocity fluctuations along the left jet (top) and right jet (bottom) across several phases for $f_o = 400$ Hz out-of-phase acoustic forcing, nonreacting flow at $U_o = 40$ m/s bulk velocity.

The top subplot of Figure 6b shows the motion of the coherent axial velocity at several different phases of the cycle in the outer left shear layer. For example, at 0° in Figure 6b (solid blue line), the maximum disturbance amplitude is at a downstream location of $x/D = 0.2$. After 115° of the cycle (solid red line) this disturbance has convected and is now at a downstream distance of $x/D = 0.6$.

The bottom portion of this figure compares the shape and amplitude of the disturbance at 0° in all four shear layers. It is evident, again from Figure 6b, that the outer left shear layer and the outer right shear layer have similar disturbance amplitudes, but are out of phase.

Figure 6c shows the coherent transverse velocity. The top and bottom subplots show the left and right jet, respectively. Again, disturbances can be seen convecting downstream, as in Figure 5. For example, the 0° line (solid blue) has a minimum value at a downstream value of $x/D = 0.4$, and this disturbance can be seen again at 115° (solid red) at a location of $x/D = 0.8$.

Several important physical mechanisms can be deduced from these series of plots. First, there is a bulk transverse motion, which is associated with the acoustic field. Second, the downstream convection of the vortical motion is evident. Third, the movement in the adjacent shear layers is out of phase in the out-of-phase forcing case. For example, the inner left shear layer and the inner right shear layer disturbances are out of phase for the axial velocity fluctuations, particularly in the region of $x/D = 0$ to $x/D = 0.3$ downstream. The opposite, in phase, behavior is also present for the in-phase forcing cases, as seen in Figure 7. In this case, the coherent vorticity disturbances have different signs, inducing opposite phase relations between the axial velocities in the adjacent shear layers, as well as the transverse velocities in the jet cores.

Data were also obtained for the reacting flow. The presence of the flame significantly changes the structure of the vortex breakdown bubble, a well-known phenomenon (Ji and Gore, 2002) that is clearly visible from Figure 4. However, the key velocity field and vorticity features discussed previously for the shear layers and annular jet core do not appear to change significantly with a flame present. To illustrate this point, the phase-resolved motion of the velocity functions is shown in Figure 8 for reacting conditions. It is important to emphasize that the same basic mechanism described for the nonreacting case is present in the reacting case, although the scales over which the development of the two shear layers proceeds is shorter in the case presented in Figure 8 because the velocity is lower.

Similar studies, including both experiment (Cala et al., 2006) and LES simulations (García-Villalba et al., 2006; Garcia-Villalba et al., 2007; Wang and Yang, 2005), have shown the propagation and eventual breakup of helical coherent structures in the swirling jet. These structures are responsible for significant wrinkling of the flame. The downstream evolution of the vortex, however, seems to be a less understood phenomenon. Whether the downstream decrease in vorticity is due to viscous decay, dilatation, vortex interaction, or some combination has yet to be finalized. Vortex interaction can lead to a shredding of the coherent structure, as can also be seen in the work by Garcia-Villalba et al. (2006).

We next consider the mass flow fluctuations for the different forcing configurations. The comparison of axial velocity between the four shear layers for the in-phase forcing shows that this forcing configuration causes in-phase fluctuations between

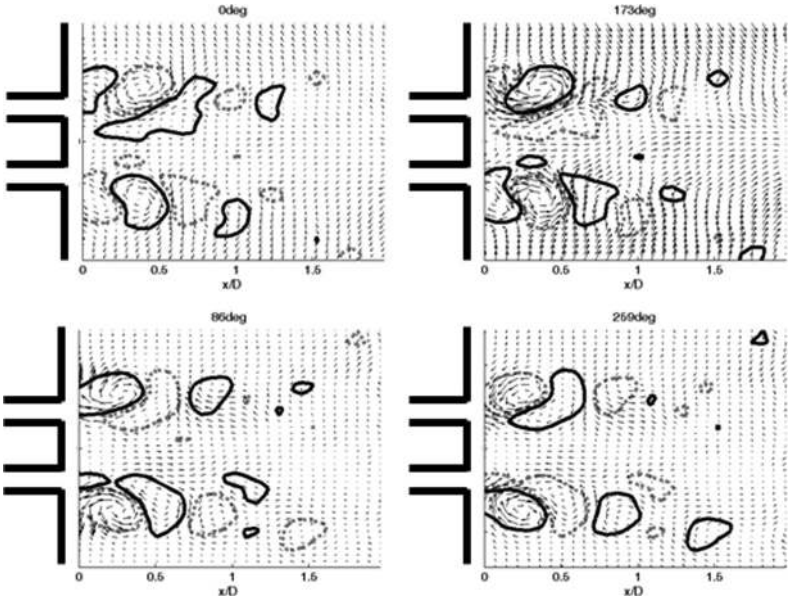


**Figure 7** Harmonically reconstructed velocity and vorticity fluctuations across several phases for $f_o = 1200$ Hz in-phase acoustic forcing, nonreacting flow at $U_o = 40$ m/s bulk velocity. The solid and dotted vorticity isocontours denote values of $\omega U_o/(r_2 - r_1) = -0.04$ and 0.04, respectively.



adjacent shear layers, while the out-of-phase case yields out-of-phase fluctuations between adjacent shear layers. This difference in shear layer response is due to the different acoustic conditions at the centerline of the annulus. The out-of-phase acoustic forcing creates a velocity antinode at the centerline of the combustor and a pressure node, causing the pressure on either side of the centerline to oscillate out of phase. Conversely, in-phase forcing creates a pressure antinode and a velocity node. The oscillating pressure field over the nozzle exit creates fluctuations in mass flow through the nozzle, which is manifested in fluctuations in the strength of the shear layer. The mass flow fluctuations on either side of the nozzle are approximately out of phase when the acoustic forcing is out of phase. Conversely, the mass flow on either side of the nozzle is in phase when the acoustic forcing is in phase. These mass flux conditions correlate with the phase of the pressure on either side of the nozzle. Mass flow fluctuations lead to vorticity fluctuations at the corner of the nozzles, as seen at the very first upstream locations. The vorticity fluctuations, initially out of phase and located at the nozzle edges, induce the out-of-phase axial velocity fluctuations in the shear layer and the convecting transverse velocity fluctuations in the jet cores.

These trends are illustrated in Figure 9, where the spatially averaged axial velocity in the left and right half of the annulus are compared between the out-of-phase and in-phase forcing cases. The phase between the axial velocities shown in Figure 9 was calculated from their Fourier transform at $f = f_o$. The estimated uncertainty in these values is 15°. The phase between the pressure on either side of the nozzle for out-of-phase acoustic forcing is 120°, and for in-phase forcing is −65°. The phase

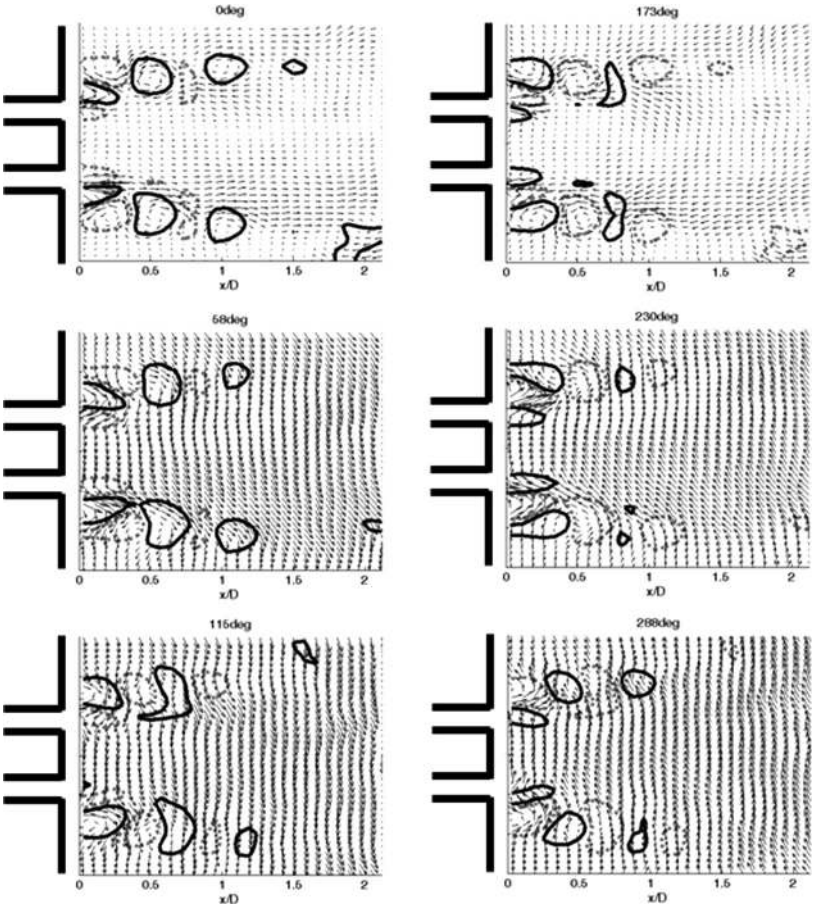


**Figure 8** Harmonically reconstructed velocity and vorticity fluctuations for $f_o = 800\,\text{Hz}$ out-of-phase acoustic forcing, reacting flow at $U_o = 10\,\text{m/s}$ bulk velocity, equivalence ratio of 0.9. The solid and dotted vorticity isocontours denote values of $\omega U_o/(r_2 - r_1) = -0.1$ and 0.1, respectively.

between the spatially averaged axial velocity on either side of the nozzle for out-of-phase forcing is 220°, and for in-phase forcing is −5°. These phases show that the acoustic forcing has a significant impact on the characteristics of the disturbance field. If the left and right sides of the burner annulus were acoustically isolated from each other, we would expect these phases to be 0° and 180°. However, because the left and right sides of the annulus are in acoustic communication with each other, which presumably would tend to equalize the pressure, these values differ from the ideal values of 0° and 180°.

The magnitudes of the average axial velocities between in- and out-of-phase forcing are very similar, despite being out of phase. The acoustic forcing amplitude in both cases is relatively constant and as such, the fluctuation amplitudes are similar. This is not the case, however, in the average transverse velocity. The out-of-phase forcing situation creates a high-amplitude sinusoidal velocity signal, while

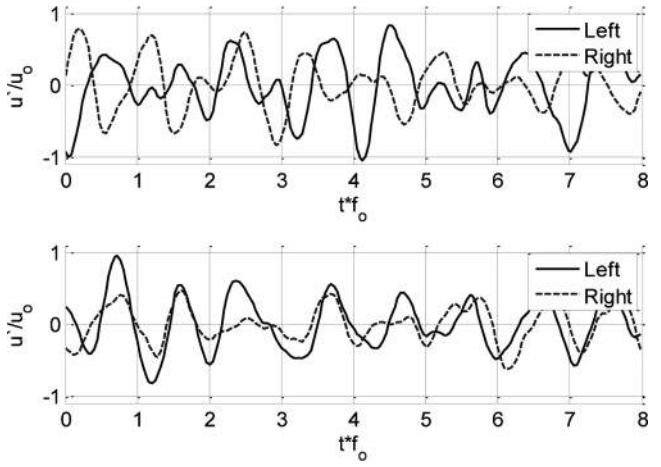


**Figure 9** Spatially averaged axial velocity fluctuations at the nozzle exit for $f_o = 400$ Hz out-of-phase acoustic forcing (top) and in-phase forcing (bottom) at $U_o = 10$ m/s nonreacting flow.



the average transverse velocity in the in-phase forcing case is much weaker, as shown in Figure 3. This data is congruent with the results discussed earlier from Staffelbach et al. (2009).

The flame is susceptible to this multidimensional disturbance field because of the stabilization of the flame in shear layers. The base of the flame experiences the longitudinal velocity fluctuations that are dominant in the shear layer as well as the vortex rollup and convection also present in the jet. Downstream, though, the flame is excited by the high amplitude transverse acoustic motion that dominates in the far field.

## CONCLUSIONS

In this work, we have analyzed the multidimensional disturbance field caused by transverse acoustic excitation of a swirling annular nozzle flow and a premixed, swirl-stabilized flame. The following conclusions can be drawn from this work.

1. The flow field near the nozzle is a superposition of acoustic and vortical disturbances, including direct transverse acoustic excitation, induced longitudinal acoustic excitation, and fluid mechanic instabilities sensitive to both longitudinal and transverse flow perturbations.
2. Different disturbance mechanisms manifest themselves in different portions of the flow. Axial velocity fluctuations are dominant in the shear layers, while transverse velocity fluctuations are dominant in the jet core.
3. Transverse acoustic excitation leads to a multidimensional velocity disturbance field. The velocity fluctuations near the base of the flame consist of both longitudinal and transverse fluctuations that are comparable in magnitude, while the velocity fluctuations farther downstream are almost completely transverse.

## ACKNOWLEDGMENTS

This work has been partially supported by the U.S. Department of Energy under contracts DEFG26-07NT43069 and DE-NT5054, with contract monitors Mark Freeman and Richard Wenglarz, respectively.

## NOMENCLATURE

$\hat{A}$ Magnitude of Fourier transform
$D$ Outer diameter of annulus
$f$ Frequency
$G$ Flame position
$H$ Centerbody height
$p$ Pressure
$p_o$ Time-averaged pressure
$\bar{p}$ Spatially averaged instantaneous pressure
$r_1$ Inner nozzle radius from centerline
$r_2$ Outer nozzle radius from centerline
$S_L$ Laminar flame speed
$t$ Time
$u$ Axial velocity
$\bar{u}$ Spatially averaged instantaneous axial velocity
$u_o$ Bulk approach velocity
$\hat{u}$ Harmonically reconstructed axial velocity
$\vec{u}$ Total velocity vector
$v$ Transverse velocity
$\bar{v}$ Spatially averaged instantaneous transverse velocity
$\hat{v}$ Harmonically reconstructed transverse velocity
$x$ Axial coordinate
$\gamma$ Ratio of specific heats
$\varphi$ Phase of Fourier transform
$\omega$ Vorticity
$\omega_o$ Time-averaged vorticity
$\hat{\omega}$ Harmonically reconstructed vorticity



## REFERENCES

Alemela, P.R., Fanaca, D., Hirsch, C., Sattelmayer, T., and Schuermans, B. 2010. Determination and scaling of thermo acoustic characteristics of premixed flames. *International Journal of Spray and Combustion Dynamics*, **2**, 169–198.

Berman, K., and Logan, S.E. 1952. Combustion studies with a rocket motor having a full-length observation window. *Jour. Am. Rocket Soc.*, **22**, 78–85.

Birbaud, A.L., Ducruix, S., Durox, D., and Candel, S. 2008. The nonlinear response of inverted "V" flames to equivalence ratio nonuniformities. *Combustion and Flame*, **154**, 356–367.

Birbaud, A.L., Durox, D., Ducruix, S., and Candel, S. 2007. Dynamics of confined premixed flames submitted to upstream acoustic modulations. *Proceedings of the Combustion Institute*, **31**, 1257–1265.

Boxx, I., Stöhr, M., Carter, C., and Meier, W. 2010. Temporally resolved planar measurements of transient phenomena in a partially pre-mixed swirl flame in a gas turbine model combustor. *Combustion and Flame*, **157**, 1510–1525.

Cala, C.E., Fernandes, E.C., Heitor, M.V., and Shtork, S.I. 2006. Coherent structures in unsteady swirling jet flow. *Experiments in Fluids*, **40**, 267–276.

Cohen, J., and Proscia, W. 2005. Characterization and control of aeroengine combustion instability: Pratt & Whitney and NASA experience. In T. Lieuwen and V. Yang (Eds.), *Combustion instabilities in gas turbine engines*, AIAAA, Washington, DC, pp. 113–146.

Davis, D.W., and Chehroudi, B. 2006. *Shear-coaxial jets from a rocket-like injector in a transverse acoustic field at high pressures*. Paper presented at the 44th Aerospace Sciences Meeting and Exhibit, Reno, NV, USA.

Ducruix, S., Schuller, T., Durox, D., and Candel, S. 2003. Combustion dynamics and instabilities: Elementary coupling and driving mechanisms. *Journal of Propulsion and Power*, **19**, 722–734.

Elias, I. 1959. Acoustical resonances produced by combustion of a fuel-air mixture in a rectangular duct. *The Journal of the Acoustical Society of America*, **31**, 296.

Ellis, M., Xia, G., Sankaran, V., Anderson, W., and Merkle, C. 2005. *Acoustic mode simulations in experimental rocket combustors*. Paper presented at the 41st Joint Propulsion Conference and Exhibit. Tuscon, AZ, USA.

García-Villalba, M., and Fröhlich, J. 2006. LES of a free annular swirling jet-Dependence of coherent structures on a pilot jet and the level of swirl. *International Journal of Heat and Fluid Flow*, **27**, 911–923.

García-Villalba, M., Fröhlich, J., and Rodi, W. 2007. Numerical simulations of isothermal flow in a swirl burner. *Journal of Engineering for Gas Turbines and Power*, **129**, 377.

Ghoniem, A., and Krishnan, A. 1989. *Origin and manifestation of flow-combustion interactions in a premixed shear layer*. Paper presented at the Twenty-second Symposium (International) on Combustion, The Combustion Institute.

Harrje, D.T., and Reardon, F.H. 1972. *Liquid propellant rocket combustion instability*. Washington, DC, Scientific and Technical Information Office, National Aeronautics and Space Administration.

Hauser, M., Lorenz, M., and Sattelmayer, T. 2010. *Influence of transversal acoustic excitation of the burner approach flow on the flame structure*. Paper presented at the ASME Turbo Expo, Glasgow, Scotland.

Hemchandra, S., and Lieuwen, T. 2010. Local consumption speed of turbulent premixed flames—an analysis of "memory effects." *Combustion and Flame*, **157**, 955–965.

Hield, P.A., Brear, M.J., and Jin, S.H. 2009. Thermoacoustic limit cycles in a premixed laboratory combustor with open and choked exits. *Combustion and Flame*, **156**, 1683–1697.

Ho, C.M., and Huang, L.S. 2006. Subharmonics and vortex merging in mixing layers. *Journal of Fluid Mechanics Digital Archive*, **119**, 443–473.

Huang, Y., Sung, H., G., Hsieh, S.Y., and Yang, V. 2003. Large-eddy simulation of combustion dynamics of lean-premixed swirl-stabilized combustor. *Journal of Propulsion and Power*, **19**, 782–794.

Huang, Y., and Yang, V. 2009. Dynamics and stability of lean-premixed swirl-stabilized combustion. *Progress in Energy and Combustion Science*, **35**, 293–364.

Ji, J., and Gore, J.P. 2002. Flow structure in lean premixed swirling combustion. *Proceedings of the Combustion Institute*, **29**, 861–867.

Karnesky, A.L., and Colucci, S.E. 1975. Recent occurrences of combustion instability in solid rocket motors—an overview. *Journal of Spacecraft and Rockets*, **12**, 33–38.

Kaskan, W.E., and Noreen, A.E. 1955. High-frequency oscillations of a flame held by a bluff body. *ASME Transactions*, **77**, 855–891.

Krebs, W., Bethke, S., Lepers, J., Flohr, P., and Prade, B. 2005. Thermoacoustic design tools and passive control: Siemens power generation approaches. In T. Lieuwen and V. Yang (Eds.), *Combustion instabilities in gas turbine engines*, AIAA, Washington, DC, pp. 89–112.

Lacarelle, A., Faustmann, T., Greenblatt, D., Paschereit, C.O., Lehmann, O., Luchtenburg, D.M., and Noack, B.R. 2009. Spatiotemporal characterization of a conical swirler flow field under strong forcing. *Journal of Engineering for Gas Turbines and Power*, **131**, 031504.

Lawn, C.J., Evesque, S., and Polifke, W. 2004. A model for the thermoacoustic response of a premixed swirl burner, Part I: Acoustic aspects. *Combustion Science and Technology*, **176**, 1331–1358.

Lieuwen, T., and Yang, V. 2005. *Combustion instabilities in gas turbine engines*. AIAA, Washington, D. C.

Macquisten, M.A., and Dowling, A.P. 1995. Combustion oscillations in a twin-stream afterburner. *Journal of Sound and Vibration*, **188**, 545–560.

Marshall, W., Pal, S., Woodward, R., Santoro, R.J., Smith, R., Xia, G., Sankaran, V., and Merkle, C.L. 2006. *Experimental and computational investigation of combustor acoustics and instabilities, Part II: Transverse modes*. Paper presented at the 44th Aerospace Sciences Meeting and Exhibit. Reno, NV.

Mongia, H.C., Held, T. J., Hsiao, G.C., and Pandalai, R.P. 2005. Incorporation of combustion instability issues into design process: GE aeroderivative and aero engines experience. In T. Lieuwen and V. Yang (Eds.), *Combustion instabilities in gas turbine engines*, AIAA, Washington, DC, pp. 43–64.

Morgans, A.S., and Stow, S.R. 2007. Model-based control of combustion instabilities in annular combustors. *Combustion and Flame*, **150**, 380–399.

O'Connor, J., Natarajan, S., Malanoski, M., and Lieuwen, T. 2010. *Disturbance field characteristics of a transversely excited annular jet*. ASME Turbo Expo 2010: Power for Land, Sea, and Air. Glasgow, Scotland.

Poinsot, T.J., Trouve, A. C., Veynante, D. P., Candel, S.M., and Esposito, E.J. 2006. Vortex-driven acoustically coupled combustion instabilities. *Journal of Fluid Mechanics*, **177**, 265–292.

Preetham, S.H., and Lieuwen, T.C. 2008. Dynamics of laminar premixed flames forced by harmonic velocity disturbances. *Journal of Propulsion and Power*, **24**, 1390–1402.

Price, E.W. 1992. Solid Rocket Combustion Instability—An American Historical Account. In L. D. Luca, E. W. Price, and M. Summerfield (Eds.), *Nonsteady burning and combustion stability of solid propellants*, AIAA, Washington, DC.

Rayleigh, L. 1896. *The theory of sound*. London, Macmillian.

Reddy, A.P., Sujith, R.I., and Chakravarthy, S.R. 2006. Swirler flow field characteristics in a sudden expansion combustor geometry. *Journal of Propulsion and Power*, **22**, 800–808.

Richecoeur, F., Scouflaire, P., Ducruix, S., and Candel, S. 2006. High-frequency transverse acoustic coupling in a multiple-injector cryogenic combustor. *Journal of Propulsion and Power*, **22**, 790–799.

Rogers, D.E., and Marble, F.E. 1956. A mechanism for high frequency oscillations in ramjet combustors and afterburners. *Jet Propulsion*, **26**, 456–462.

Schadow, K.C., and Gutmark, E. 1992. Combustion instability related to vortex shedding in dump combustors and their passive control. *Progress in Energy and Combustion Science*, **18**, 117–132.

Schuermans, B., Paschereit, C., and Monkiewitz, P. 2006. *Nonlinear combustion instabilities in annular gas-turbine combustors*. Paper presented at the 44th AIAA Aerospace Sciences Meeeting and Exhibit, Reno, NV, USA.

Schwieger, R.G. 2007. *Combined cycle journal*. Las Vegas, NV, PSI Media.

Sewell, J., and Sobieski, P. 2005. Monitoring of combustion instabilities: Calpine's experience. In T. Lieuwen and V. Yang (Eds.), *Combustion instabilities in gas turbine engines*, AIAA, Washington, DC, pp. 147–162.

Shtork, S.I., Vieira, N.F., and Fernandes, E.C. 2008. On the identification of helical instabilities in a reacting swirling flow. *Fuel*, **87**, 2314–2321.

Smith, K., and Blust, J. 2005. Combustion instabilities in industrial gas turbines: Solar turbines' experience. In T. Lieuwen and V. Yang (Eds.), *Combustion instabilities in gas turbine engines*, AIAA, Washington, DC, pp. 29–42.

Staffelbach, G., Gicquel, L.Y., Boudier, M.G., and Poinsot, T. 2009. Large eddy simulation of self excited azimuthal modes in annular combustors. *Proceedings of the Combustion Institute*, **32**, 2909–2916.

Stow, S.R., and Dowling, A.P. 2001. *Thermoacoustic oscillations in an annular combustor*. Paper presented at the ASME Turbo Expo, New Orleans, LA, USA.

Syred, N. 2006. A review of oscillation mechanisms and the role of the precessing vortex core (PVC) in swirl combustion systems. *Progress in Energy and Combustion Science*, **32**, 93–161.

Thumuluru, S.K., Bobba, M.K., and Lieuwen, T. 2007. *Mechanism of the nonlinear response of a swirl flame to harmonic excitation*. Paper presented at the ASME Turbo Expo 2007: Power for Land, Sea and Air. Montreal, Canada.

Thumuluru, S.K., and Lieuwen, T. 2009. Characterization of acoustically forced swirl flame dynamics. *Proceedings of the Combustion Institute*, **32**, 2893–2900.

Venkataraman, K.K., Preston, L., H., Simons, D., W., Lee, B., J., Lee, J.G., and Santavicca, D. 1999. Mechanism of combustion instability in a lean premixed dump combustor. *Journal of Propulsion and Power*, **15**, 909–918.

Wang, S., and Yang, V. 2005. Unsteady flow evolution in swirl injectors with radial entry. II. External excitations. *Physics of Fluids*, **17**, 045107.

Wolf, P., Staffelbach, G., Roux, A., Gicquel, L., Poinsot, T., and Moureau, V. 2009. Massively parallel LES of azimuthal thermo-acoustic instabilities in annular gas turbines. *Comptes Rendus Mecanique*, **337**, 385–394.